Separation and Purification Technology xxx (2015) xxx–xxx

Contents lists available at ScienceDirect

Separation and Purification Technology

journal homepage: www.elsevier.com/locate/seppur

Facile synthesis of zirconia doped hybrid organic inorganic silica membranes

Marcel ten Hove, Arian Nijmeijer, Louis Winnubst *

Inorganic Membranes, MESA+ Institute for Nanotechnology, University of Twente, P.O. Box 217, 7500 AE Enschede, The Netherlands

ARTICLE INFO

Article history:
Received 8 September 2014
Received in revised form 5 December 2014
Accepted 19 December 2014
Available online xxxx

Keywords:
Gas separation
Hybrid silica
Metal doping
Sol–gel

ABSTRACT

Hybrid organic inorganic silica membranes are interesting candidates for gas-separation applications due to their excellent hydrothermal stability. However, up to now these membranes lack the separation performance required to separate hydrogen from carbon dioxide. In this work a procedure for doping zirconia into the hybrid silica matrix is reported, resulting in an improved H_2/CO_2 permselective membrane compared with non-doped hybrid silica membranes. Zirconia doped 1,2-bis(triethoxysilyl)ethane (Zr-BTESE) was synthesized by sol–gel chemistry, using zirconyl nitrate as the zirconium source. By optimization of the sol reaction conditions (i.e. reaction time and temperature) a homogenous sol was obtained. Defect-free membranes were obtained by adjusting the concentration of the dip-coating solution. The doped membranes showed a slight decrease in hydrogen permeance from 4.4×10^{-7} to 1.8×10^{-7} mol m^{-2} s^{-1} Pa^{-1} as compared to an undoped BTESE membrane, but a large increase in H_2/CO_2 (from 4 to 16) and H_2/N_2 (from 12 to 100) permselectivity was observed.

1. Introduction

The world energy demand is increasing and although the growth in energy produced by renewable sources is large, there is still a big demand for energy from coal and gas, according to the energy outlook of the EIA [1]. This demand for fossil fuels will cause a further increase in carbon dioxide emissions. According to the 4th IPCC assessment report carbon dioxide is one of the main contributors to global warming [2]. It is therefore necessary to reduce the emissions of CO_2 by means of carbon capture and storage (CCS). One of the strategies for CCS is pre-combustion carbon capture in which a fuel is converted to hydrogen and carbon dioxide that can be separated easily.

Methane steam reforming (MSR), as given in reaction (1) can be utilized to convert natural gas to hydrogen and carbon monoxide, a mixture called synthesis gas or syngas. This syngas is shifted towards hydrogen and carbon dioxide in the water gas shift reaction (WGS) (2). Due to the highly exothermic nature of the WGS reaction it is often performed in a two-stage approach to ensure full conversion of carbon monoxide to hydrogen and CO_2 [3]. A typical purification step to obtain 90% pure hydrogen for pre-combustion carbon capture is physical absorption of carbon dioxide, e.g. by using Selexol and Rectisol [4]. For applications that demand high purity hydrogen like ammonia synthesis or fuel cell applications typically pressure swing adsorption is used [3].

$$CH_4 + H_2O \rightleftharpoons 3H_2 + CO \quad \Delta H = 206 kJ/mol \tag{1}$$

$$CO + H_2O \rightleftharpoons CO_2 + H_2 \quad \Delta H = -41 kJ/mol \tag{2}$$

By using a water gas shift membrane reactor (WGS-MR) instead of the conventional approach, the equilibrium of the WGS reaction (2) can be shifted to the product (H_2 and CO_2) side by continuous removal of hydrogen. The need for extra cooling steps is eliminated by the integration of reaction and separation into one unit operation. This reduces the energy demand, resulting in a more efficient process.

Membranes that are utilized in a WGS-MR need to have a high hydrogen permeance and a high H_2/CO_2 selectivity. Palladium membranes have a high H_2/CO_2 selectivity and high hydrogen permeance, but suffer from hydrogen embrittlement and sulfur poisoning, which decreases their lifespan [5]. On the other hand sol–gel derived silica membranes are known for their excellent H_2/CO_2 selectivity, but degrade in a hydrothermal environment due to the mobility of the silanol groups in the material [6,7]. Strategies to increase the hydrothermal stability of silica are doping silica with metal oxides to stabilize the siloxane bonds [6,8–11] or by using a hydrophobic compound to prevent water sorption onto or into the material [12–14]. The latter approach is used in hybrid silica membranes based on bridged silsesquioxanes like

* Corresponding author. Tel.: +31 534982994.
E-mail address: a.j.a.winnubst@utwente.nl (L. Winnubst).

http://dx.doi.org/10.1016/j.seppur.2014.12.033
1383-5866/

bis(triethoxysilyl)ethane (BTESE). It is proven that BTESE membranes are hydrothermally stable for over one year in dehydration of butanol by pervaporation at 150 °C [15]. These BTESE derived membranes have a lower H_2/CO_2 selectivity than silica membranes. Kanezashi et al. [16] proposed that the network of BTESE is more loose due to the ethane bridge, which would lead to a larger pore size. From silica it is known that an increase in calcination temperature from 400 °C to 600 °C leads to densification of the matrix and a lower number of silanol groups, which leads to an increase in H_2/CO_2 selectivity from 7.5 to 71 [17]. Since BTESE starts to decompose above 470 °C in an inert atmosphere [12] only temperatures below this decomposition temperature can be used for calcination. Typical calcination temperatures for BTESE are 300 °C [12,16], which leads to a less condensed network and hence to a lower H_2/CO_2 selectivity if compared with silica membranes calcined at 600 °C.

In order to increase the gas separation performance of these hybrid silica systems two routes have been suggested. The first route is changing the length of the organic bridge in the silsesquioxane [18], while the second route is metal doping of the hybrid silica matrix [19]. Metal doping of silica with niobium, cobalt or nickel was used by several research groups to improve the hydrothermal stability [9,11,20–24] and was only recently used on BTESE to improve the gas separation performance. Qi et al. doped BTESE with niobia to achieve a H_2/CO_2 selectivity of 200 [19]. The authors explained this improved selectivity by network densification, caused by niobia, and by a reduced affinity for CO_2 due to the presence of acidic niobia groups in the niobia/BTESE network.

Zirconia doping of silica by using a zirconium-alkoxide was done by Yoshida et al. [24]. They observed that increasing the zirconia content in silica results in increased activation energy of permeation for helium and hydrogen. This increased activation energy is ascribed to network densification, which leads to smaller pore sizes. This results in lower gas permeances but also in a higher selectivity for hydrogen over carbon dioxide.

In this work a zirconia doped hybrid silica sol was produced by using zirconyl nitrate as a zirconium source. Zirconyl nitrate was chosen instead of a zirconium-alkoxide precursor due to the too fast hydrolysis rate of the latter. Membranes were prepared by dip coating of the sol on a porous support. The effects of sol concentration in the dip coat solution on membrane microstructure and membrane performance were investigated. The results are compared with undoped BTESE membranes fabricated in a similar way.

2. Experimental

2.1. Sol–gel preparation

All chemicals were used as received. The hybrid silica precursor, 1,2-bis(triethoxysilyl)ethane (BTESE 97%), was obtained from ABCR. A zirconyl nitrate solution ($ZrO(NO_3)_2$ (99%, 35 wt.% in dilute nitric acid) was obtained from Sigma–Aldrich. Ethanol (99%) and concentrated nitric acid (65%) were obtained from Merck.

BTESE sols were prepared by the following procedure: 1.04 mL of a 1.77 mol/L HNO_3 solution was added to 5.53 mL ethanol and placed in an ice bath. Subsequently 3.33 mL of BTESE was dropped slowly into the mixture under vigorous stirring to obtain a final ratio of BTESE:EtOH:HNO_3:H_2O of 1:10.8:0.2:6. The mixture was reacted at 60 °C for 90 min and put in an ice bath to quench the reaction. Ethanol was added to the solution to dilute the sol for dip coating to a final silicon concentration of 0.3 mol/L.

Zirconia doped BTESE sols were made by the following procedure: zirconyl nitrate (0.802 mL), 0.337 mL H_2O and 5.53 mL ethanol were mixed and the mixture was placed in an ice bath. BTESE (3.33 mL) was added drop wise to the mixture under vigorous stirring to obtain a final ratio of BTESE:$ZrO(NO_3)_2$:EtOH:HNO_3:H_2O of 1:0.19:10.5:0.2:6. The mixture was reacted at 25 °C for 90 min and afterwards put in an ice bath to quench the reaction. Ethanol was added to the solution to dilute the sol for dip coating. Final [Zr + Si] concentrations were 0.33 mol/L, 0.2 mol/L and 0.13 mol/L with a Si:Zr ratio of 10:1. All sol solutions were stored at −18 °C prior to further use.

2.2. Characterization

The sol particle size was determined by dynamic light scattering (DLS) using a Malvern Zetasizer Nano ZS. Diluted sols were used for the measurements and were filtered over a 0.2 μm filter beforehand to remove dust-particles that could have a negative influence on the measurement.

Unsupported membrane materials were obtained by drying the sol overnight in a petri dish. After drying, the flakes were calcined under nitrogen. Calcination was performed at 400 °C or 600 °C with a heating/cooling rate of 0.5 °C/min and a dwell of 3 h. After calcination the flakes were ground into a powder using a mortar. Unsupported silica, prepared by the procedure as described by De Vos and Verweij [17], was used for comparison. These powders were calcined at 600 °C in air with a heating/cooling rate of 0.5 °C/min and a dwell of 3 h.

Nitrogen adsorption experiments were performed on unsupported membrane materials with a Quantachrome Autosorb-1MP. The samples were degassed overnight at 300 °C. The surface area of the samples was calculated using the BET equation and the micropore volume was calculated using the Dubinin–Radushkevich method [25]. Powder X-ray diffraction was performed on a Bruker Phaser D2. Scans were taken from 2θ of 20° to 80° with a step size of 0.02° and a step time of 0.5 s. Thermogravimetric analysis was performed on a Netzch STA 449 F3 Jupiter with a nitrogen flow of 70 ml min^{-1}. Measurements were taken with a heating rate of 20 °C/min from 35 °C to 1000 °C. Pretreatment was done at 50 °C in vacuum to ensure that most of the physisorbed water is removed.

2.3. Membrane preparation

Porous α-alumina supports (pore size 80 nm, porosity 35%) with a diameter of 39 mm and a thickness of 2 mm (Pervatech B.V. the Netherlands) were coated twice under cleanroom conditions with a boehmite sol and calcined at 650 °C at a heating rate of 1 °C/min and a dwell of 3 h, resulting in a γ-alumina intermediate layer with a thickness of 3 μm and a pore size of 5 nm as reported by Uhlhorn et al. [26]. BTESE and Zr-BTESE layers were coated in one step under cleanroom conditions onto the supported γ-alumina membranes using an automatic dip-coating machine, with an angular dipping rate of 0.06 rad s^{-1}. The membranes were calcined under nitrogen at 400 °C with a heating and cooling rate of 0.5 °C/min and a dwell of 3 h. Zr-BTESE membranes were named Zr-BTESE-X in which X is the total [Si + Zr] concentration in mol/L in the dip coating solution.

High resolution scanning electron microscopy (SEM) was performed with a Zeiss Leo 1550 FESEM on membrane cross-sections to determine the thickness of the selective layer. The cross sections were placed on a sample holder and partly covered with aluminum tape to prevent sample charging. No further pretreatment was done on the samples and images were acquired at an accelerating voltage of 1 kV.

2.4. Single gas permeation

The membrane performance was characterized by means of single gas permeation. The membranes were measured in a

Please cite this article in press as: M. ten Hove et al., Facile synthesis of zirconia doped hybrid organic inorganic silica membranes, Separ. Purif. Technol. (2015), http://dx.doi.org/10.1016/j.seppur.2014.12.033

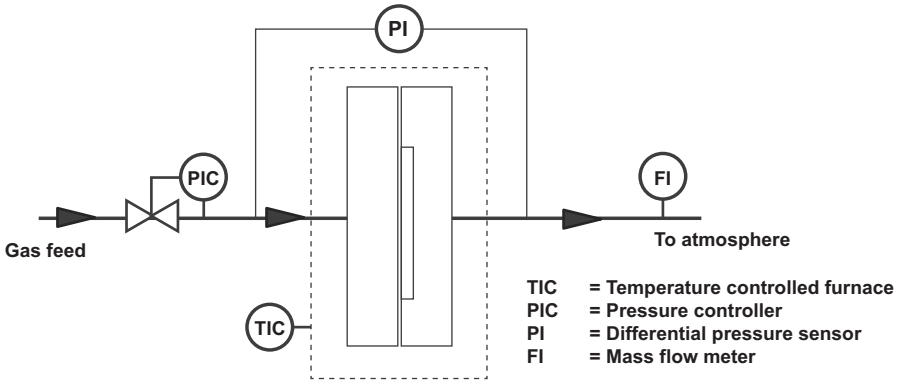

Fig. 1. Schematic representation of the single gas permeation setup.

"dead-end" mode as depicted in Fig. 1. A feed pressure of 3 bara was applied to the membrane, while the permeate pressure was kept atmospheric. The pressure difference over the membrane was measured by a differential pressure sensor (GE Druck STX2100). The flow through the membrane was determined by a Bronkhorst EL-FLOW mass flow meter.

The membranes were pretreated by heating up to 200 °C with a heating rate of 1.5 °C/min under helium flow to ensure a complete removal of water from the membranes. After this conditioning step, the following gases were measured (in order of measurement): He, N_2, CH_4, H_2, and CO_2. All gases were equilibrated for at least half an hour to ensure a constant flux. Two membranes were made from each sol and gas permeation results were averaged over the two membranes. The difference between the two membranes measured was within the experimental error.

3. Results

3.1. Sol characteristics

Initially a sol synthesis of Zr-BTESE was performed at 60 °C, using the same experimental conditions as for the undoped BTESE sol synthesis. These conditions resulted in gelation of the Zr-BTESE system within 10 min, which was caused by the high reactivity of the zirconium precursor. At a lower reaction temperature of 25 °C the overall rate of the reaction was decreased, resulting in a non-gelated system with a monomodal sol particle size of 6.5 nm after 90 min of reaction.

In Fig. 2 the size intensity distribution are shown from the dynamic light scattering results for silica, BTESE and Zr-BTESE sol particles. The Zr-BTESE sol synthesized at 25 °C has a similar polydispersity as the silica sol synthesized at 60 °C, both showing a lower polydispersity compared to pure BTESE synthesized at 60 °C. The average particle size of the silica, BTESE and Zr-BTESE sols are 5.6, 10.2 and 6.5 nm respectively. Besides these sols a BTESE sol was synthesized at a reaction temperature of 30 °C for 90 min. This sol yielded an average sol particle size of 3.6 nm, which is smaller than the pore size of 5 nm of the γ-alumina substrate. Hence this BTESE sol was not suitable for coating and further membrane fabrication.

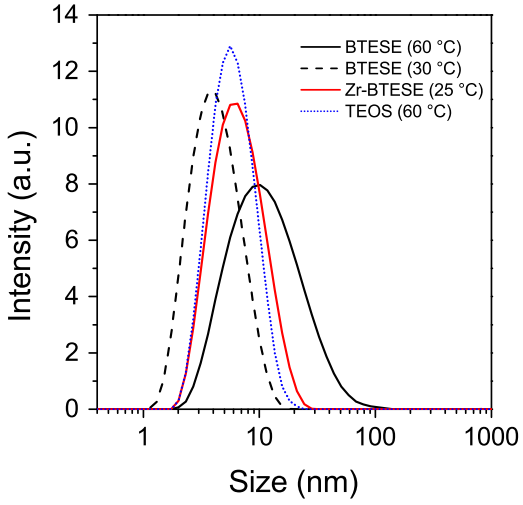

Fig. 2. Dynamic light scattering intensity of the particles in the produced sols. The value in brackets is the temperature during the sol synthesis.

3.2. Powder characteristics

Fig. 3 shows the nitrogen adsorption isotherms for calcined silica, BTESE and Zr-BTESE. They have a type 1 isotherm, which corresponds to microporous materials. In Table 1 the calculated micropore volume and surface area of the prepared materials are given. BTESE shows a high surface area and micropore volume,

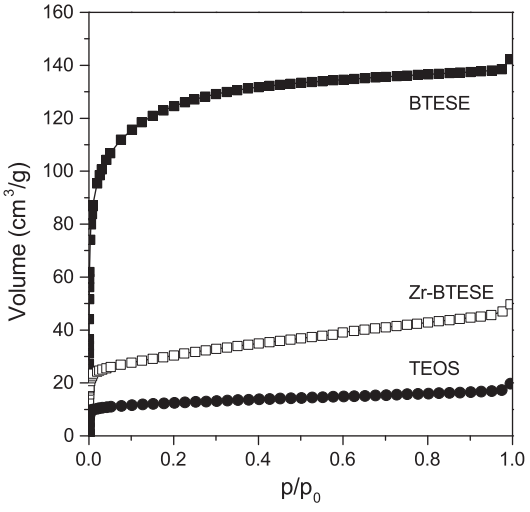

Fig. 3. Nitrogen adsorption isotherms for unsupported membranes.

485 m^2/g and 0.173 cm^3/g respectively, while silica has a low surface area and micropore volume of respectively 46 m^2/g and 0.022 cm^3/g. Zr-BTESE shows a lower surface area and micropore

Please cite this article in press as: M. ten Hove et al., Facile synthesis of zirconia doped hybrid organic inorganic silica membranes, Separ. Purif. Technol. (2015), http://dx.doi.org/10.1016/j.seppur.2014.12.033

Table 1
Micropore volume and surface area for unsupported membranes as determined by nitrogen adsorption. The temperature between brackets corresponds to the calcination temperature.

	Micropore volume (cm^3/g)	Surface area (m^2/g)
BTESE (400 °C)	0.173	485
Zr-BTESE (400 °C)	0.055	154
TEOS (600 °C)	0.022	46

volume as compared to BTESE, indicating that zirconia doping indeed results in a denser structure.

Fig. 4 shows the XRD pattern of BTESE calcined at 400 °C and Zr-BTESE calcined at 400 °C and 600 °C. The peak at 51° 2θ, as visible in all XRD patterns, can be ascribed to a small defect in the nickel shield of the apparatus. In all patterns no crystalline peaks were detected, while only broad bands are found, which are typical for randomly-oriented amorphous systems. The patterns for BTESE and Zr-BTESE calcined at 400 °C and 600 °C are similar, which is an indication that the zirconia is fully incorporated and does not segregate into crystalline clusters that would be detectable by XRD.

Fig. 5 shows the results of the thermogravimetric analysis. Due to the pretreatment of the sample no significant loss as a result of water evaporation is observed. The first part of the mass loss, up till 250 °C, is the removal of strongly bound water and the decomposition of nitrates. For Zr-BTESE the weight loss is bigger in this part due to the higher amount of nitrates present from the zirconyl nitrate precursor. After this initial mass loss, both BTESE and Zr-BTESE follow the same trend. The trend found is in line with the thermogravimetric graphs as described by Kappert et al. [27]

3.3. Membrane characteristics

In Fig. 6 a SEM cross-section is given of a Zr-BTESE-0.2 membrane. The α-alumina substrate, the γ-alumina intermediate layer and the Zr-BTESE top layer are clearly visible. No pore intrusion of the sol into the intermediate layer is observed. Table 2 provides the thickness of all membrane separation layers investigated, as determined from SEM images. The BTESE-0.3 and Zr-BTESE-0.33 have the same degree of dilution from the starting sol and hence have the same silicon concentration. However due to the addition of zirconium the total [Si + Zr] concentration is increased. This increase in metal-ion concentration is reflected in the measured thickness, as the BTESE-0.3 and Zr-BTESE-0.33 have a thickness of 270 and 300 nm respectively.

Fig. 7 shows the gas permeance measured at 200 °C at a transmembrane pressure of 2 bar as function of the kinetic diameter of the gas molecules for BTESE membranes with a dip sol concentration of 0.3 mol/L and Zr-BTESE membranes with a dip sol concentration of 0.33 mol/L, 0.2 mol/L and 0.13 mol/L. Table 3 shows the hydrogen permeances of these membranes and the permselectivities (F_α) of hydrogen over carbon dioxide, nitrogen and methane respectively. The hydrogen permeance for BTESE-0.3 is 4.4×10^{-7} mol m^{-2} s^{-1} Pa^{-1} with a H_2/N_2 selectivity of 12, which is an indication that molecular sieving is prevailing for these membranes.

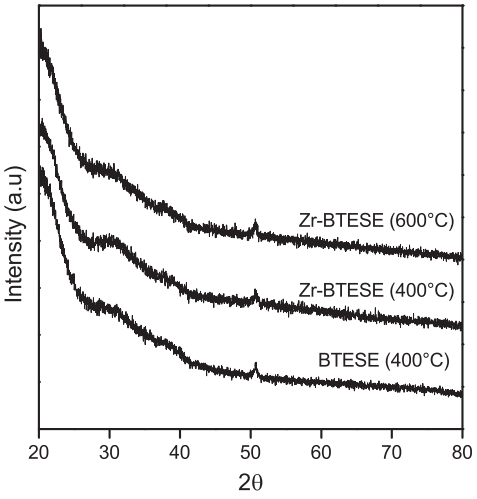

Fig. 4. XRD patterns of BTESE calcined at 400 °C and Zr-BTESE calcined at 400 °C and 600 °C. The band for amorphous silica is visible at 30° 2θ. The peak at 51° 2θ is due to an instrument error.

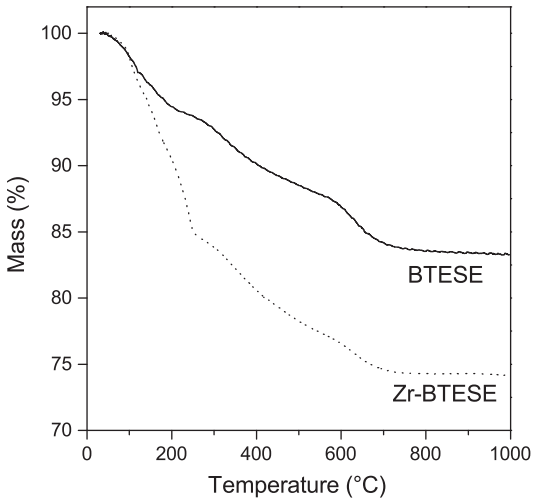

Fig. 5. Thermogravimetric curve of BTESE and Zr-BTESE powders at a heating rate of 20 °C min^{-1} and nitrogen flow of 70 mL min^{-1}.

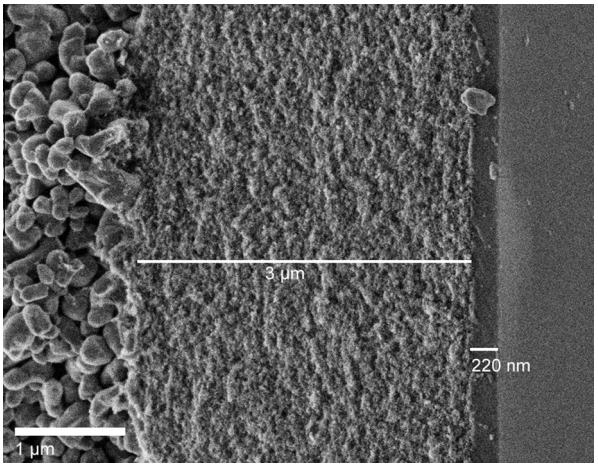

Fig. 6. SEM picture of Zr-BTESE-0.2 membrane. The α-Al_2O_3 support layer, γ-Al_2O_3 intermediate layer and hybrid silica top layer are all clearly visible.

Table 2
Layer thickness of membranes as determined from SEM images.

Membrane	Layer thickness (nm)
BTESE-0.3	270 ± 17
Zr-BTESE-0.33	300 ± 20
Zr-BTESE-0.20	220 ± 13
Zr-BTESE-0.13	148 ± 8

Please cite this article in press as: M. ten Hove et al., Facile synthesis of zirconia doped hybrid organic inorganic silica membranes, Separ. Purif. Technol. (2015), http://dx.doi.org/10.1016/j.seppur.2014.12.033

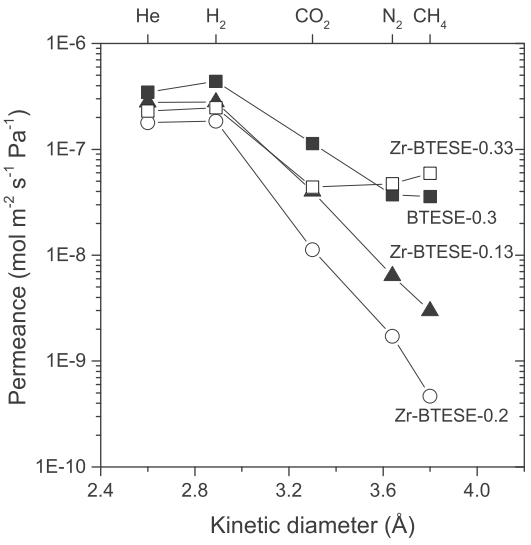

Fig. 7. Gas permeance versus kinetic diameter for the membranes coated with a different sol dilution measured at 200 °C with a transmembrane pressure of 2 bar.

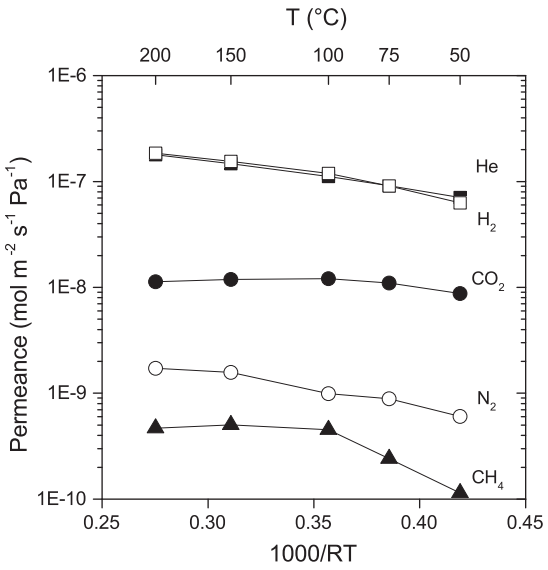

Fig. 8. Arhenius plot for the Zr-BTESE-0.2 membrane with a transmembrane pressure of 2 bar.

Table 3
Hydrogen permeance and permselectivity, F_α, of H_2/CO_2 and H_2/N_2 for membranes, measured at 200 °C with a transmembrane pressure of 2 bar.

	H_2 permeance (10^{-7} mol m^{-2} s^{-1} Pa^{-1})	F_α H_2/CO_2	F_α H_2/N_2	F_α H_2/CH_4
Knudsen		4.7	3.7	2.8
BTESE-0.3	4.4	4	12	12
Zr-BTESE-0.33	1.9	6	5	4
Zr-BTESE-0.20	1.8	16	100	400
Zr-BTESE-0.13	2.8	7	44	94

Table 4
Apparent activation energies for Zr-BTESE and BTESE.

Gas	E_{app} (kJ/mol)	
	Zr-BTESE-0.2	BTESE [18]
He	6.4 ± 0.3	1.7
H_2	7.4 ± 0.7	0.9
CO_2	1.5 ± 1.0	−2.4
N_2	7.4 ± 0.8	0.6
CH_4	9.5 ± 3.3	0.5

These values are in accordance to results obtained in previous work[28]. The addition of zirconium to the BTESE matrix leads to a slightly lower permeance for helium and hydrogen, compared to undoped BTESE. The Zr-BTESE-0.33 membrane, which was only slightly thicker than the BTESE-0.3 membrane, showed cracks after post analysis Rhodamine staining. This proves that the observed gas transport through the Zr-BTESE-0.33 membranes was governed by defects in the membrane. Zr-BTESE membranes with lower dip sol concentrations and hence thinner layers show an increase in the selectivity of hydrogen over the other gases. For Zr-BTESE-0.2 the H_2/CO_2 selectivity has increased from 4 to 16 while the H_2/N_2 selectivity has increased from 12 to 100 if compared with BTESE. The Zr-BTESE-0.13 shows selectivity for H_2/CO_2 and H_2/N_2 of 7 and 44 respectively with a hydrogen permeance of 2.8×10^{-7} mol m^{-2} s^{-1} Pa^{-1}.

The temperature dependency for the Zr-BTESE-0.2 membrane is measured in the temperature range of 50–200 °C. In Fig. 8 the permeance is plotted against 1000/RT. Table 4 shows the calculated apparent activation energy of permeation for each gas Zr-BTESE and the reported values for BTESE [18]. The apparent activation energy of permeation for hydrogen is 7.4 kJ/mol, which is almost eight times higher than reported for BTESE.

4. Discussion

Miller and Ko [29] state that for a mixed-metal oxide sol a more homogenous structure on the atomic scale can be achieved if the reaction rate of the individual metal precursors is low. This approach results in a true mixed oxide system, rather than clusters of the faster reacting species in a matrix of the slower reacting ones. The zirconyl nitrate precursor is the faster reacting component compared to BTESE, which results in fast gelation during sol synthesis at 60 °C when using a mixture of these two precursors, while a well-defined sol is obtained under the same reaction conditions when only the BTESE precursor is used. Lowering the reaction temperature for the mixed metal oxide system from 60 °C to 25 °C results in the formation of a sol with a uniform particle size distribution instead of a gel. It is assumed that a more uniform particle size distribution results in the formation of a more homogeneous separation layer with a better separation performance.

XRD shows no crystalline domains of zirconia. This gives an indication that the zirconia is incorporated into the silica matrix or exist in (nanometer or sub-nanometer sized) domains that are smaller than the detection limit for XRD. For amorphous zirconia a broad band would be expected at 30° and 50° [30]. Even when the powder is calcined at 600 °C, which is above the decomposition temperature of BTESE and above the crystallization temperature from amorphous to tetragonal zirconia [31], still no crystalline peaks appear. Apart from the higher nitrate content no significant differences in the decomposition of the ethane bridge between undoped and zirconia doped BTESE is observed. Kappert et al. [27] observed after accurate kinetic analysis that the decomposition of the ethane linker starts at 500 °C, which implies that firing at 400 °C is possible without risk of degradation.

The micropore volume and surface area as analyzed from nitrogen adsorption measurements can be correlated to membrane performance. Based on the gas permeation results of de Vos et al. [17] on silica membranes, calcined at 600 °C, one can conclude that the average pore size of the silica membrane is smaller than the kinetic

Please cite this article in press as: M. ten Hove et al., Facile synthesis of zirconia doped hybrid organic inorganic silica membranes, Separ. Purif. Technol. (2015), http://dx.doi.org/10.1016/j.seppur.2014.12.033

diameter of nitrogen. Therefore only a small amount of pores can be probed by nitrogen during the nitrogen adsorption experiments, which leads to the observed small micropore volume and surface area for the silica system (see Table 1). For BTESE an almost ninefold larger surface area and micropore volume is found than for silica. This indicates that more pores are accessible for nitrogen, which is reflected in the high nitrogen flux of BTESE. For Zr-BTESE a lower micropore volume and surface area is observed compared to BTESE, but not as small as for silica calcined at 600 °C. From these results it can be assumed that the addition of zirconia in BTESE leads to a (micro) porous structure, which is less accessible for nitrogen than in the case of undoped BTESE.

The Zr-BTESE-0.2 and Zr-BTESE-0.13 membranes are thinner than the undoped BTESE membrane, but have a lower permeance for helium and hydrogen in comparison with undoped BTESE. Besides, the selectivity of these gases towards CO_2, N_2 and CH_4 were largely increased. The higher permselectivity indicate that the pore size of the membrane is smaller in comparison with BTESE, which corresponds well with the sorption data on unsupported membrane material. This shows that the sorption data on unsupported membrane material can be used as an indication of the membrane performance. The activation energy of permeation is often a good measure for the pore size as it correlates to the energy of diffusion through the pores [24,32]. The activation energies of permeation are in general much higher for Zr-BTESE-0.2 in comparison with BTESE [18], which is another indication that the pore size for Zr-BTESE is smaller in comparison with BTESE. Also for the larger gases the activation energy is much larger, which is a clear indication that the pore size becomes much smaller upon doping with zirconia. Also CO_2 shows positive activation energy, while for BTESE the activation energy is negative. This negative activation energy for CO_2 transport through BTESE membranes is ascribed to the fact that there is a strong affinity for CO_2. Therefore CO_2 transport is governed by molecular affinity rather than by size, which gives rise to H_2/CO_2 permselectivities which are lower than the Knudsen value [18].

BTESE membranes without defects and with a thickness of up to 550 nm have been reported [28,33]. However, the here prepared Zr-BTESE-0.33 membranes with a thickness of 300 nm show already defects. There are a number of factors that could explain this behavior. First of all the smaller particle size of the Zr-BTESE sol can lead to higher inter-particle stresses during drying [34]. Another factor could be that the zirconia is forming small clusters in the matrix with a higher coordination number. These small clusters, with a size of around 0.4 nm, and hence undetectable by XRD, are known to be formed under aqueous conditions [35]. These clusters can give rise to a more rigid structure, leading to higher drying stresses.

In Fig. 9 the single gas permeance of BTESE-0.3 and Zr-BTESE-0.2 are compared with literature values for Nb-BTESE [36], TEOS-derived silica [17], Co-TEOS [37] and Zr-TEOS [24]. TEOS-derived silica outperforms all other membranes with respect to hydrogen permeance and H_2/CO_2 permselectivity, but is known to be unstable under steam conditions [7]. Co-TEOS has the highest H_2/CO_2 selectivity, but the hydrogen permeance is too low to be attractive for an application. Zr-BTESE shows in comparison to Zr-TEOS similar hydrogen permeance, but a much better selectivity with respect to the other gases. Although some general comparisons can be made between literature data, a true comparison is not possible, since there are differences in the used substrate, coating method and measurement method.

A H_2/CO_2 selectivity of 16 as achieved in this work is not sufficient for WGS-MR applications, since it would lead to a too high CO_2 concentration that is emitted. However, we show that the pore size of BTESE can be tuned towards a better selectivity of H_2/CO_2 without compromising too much on hydrogen permeance.

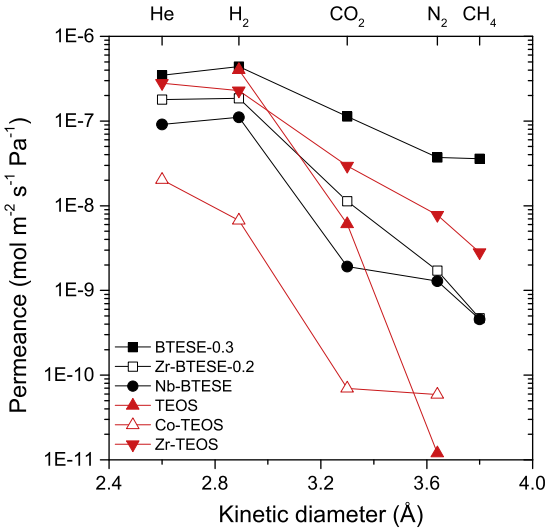

Fig. 9. Comparison of BTESE and Zr-BTESE with Nb-BTESE [36], TEOS [17], Co-TEOS [37] and Zr-TEOS [24].

5. Conclusion

Zirconia doped BTESE membranes have been successfully synthesized by a sol–gel method, using zirconyl nitrate and 1,2-bis(triethoxysilyl)ethane (BTESE) as precursors. By using a reaction temperature of 25 °C a homogenous sol has been produced that shows no crystalline zirconia in XRD-spectra after calcination at 400 °C or 600 °C in nitrogen. These Zr-doped BTESE membranes have a slightly lower permeance for the gases He and H_2 if compared with BTESE-derived membranes but an increase in selectivity of hydrogen over carbon dioxide, nitrogen and methane is achieved. A Zr-BTESE membrane has a hydrogen permeance of $1.8 \cdot 10^{-7}$ mol m^{-2} s^{-1} Pa^{-1}, and H_2/CO_2, H_2/N_2 and H_2/CH_4 permselectivity of respectively 16, 100 and 400.

Nitrogen adsorption analysis indicates a threefold decrease in micropore volume and micropore surface area for Zr-doped BTESE with respect to undoped BTESE indicating a micropore structure for Zr-BTESE, which is less accessible for nitrogen than the micropore structure of undoped BTESE. Gas adsorption on unsupported membrane materials can give a reasonable indication of the membrane performance of such materials.

Acknowledgements

We acknowledge financial support for this research from ADEM, A green Deal in Energy Materials of the Ministry of Economic Affairs of The Netherlands (www.adem-innovationlab.nl).

References

[1] International Energy Outlook 2010, in: U.S. Energy Information Administration, 2010.
[2] S. Solomon, D. Qin, M. Manning, Z. Chen, M. Marquis, K.B. Averyt, M. Tignor, H.L. Miller, IPCC, 2007: Climate Change 2007: The Physical Science Basis, Cambridge University Press, 2007.
[3] P. Häussinger, R. Lohmüller, A.M. Watson, Hydrogen, in: Ullmann's Encyclopedia of Industrial Chemistry, Wiley-VCH Verlag GmbH & Co. KGaA, 2000.
[4] J. Black, Cost and Performance Baseline for Fossil Energy Plants: Volume 1: Bituminous Coal and Natural Gas to Electricity, 2010.
[5] F. Gallucci, E. Fernandez, P. Corengia, M. van Sint Annaland, Recent advances on membranes and membrane reactors for hydrogen production, Chem. Eng. Sci. 92 (2013) 40–66.
[6] V. Boffa, D.H.A. Blank, J.E. ten Elshof, Hydrothermal stability of microporous silica and niobia–silica membranes, J. Membr. Sci. 319 (2008) 256–263.

[7] M.C. Duke, J.C.D. da Costa, D.D. Do, P.G. Gray, G.Q. Lu, Hydrothermally robust molecular sieve silica for wet gas separation, Adv. Funct. Mater. 16 (2006) 1215–1220.
[8] M. Asaeda, Y. Sakou, J. Yang, K. Shimasaki, Stability and performance of porous silica–zirconia composite membranes for pervaporation of aqueous organic solutions, J. Membr. Sci. 209 (2002) 163–175.
[9] R. Igi, T. Yoshioka, Y.H. Ikuhara, Y. Iwamoto, T. Tsuru, Characterization of co-doped silica for improved hydrothermal stability and application to hydrogen separation membranes at high temperatures, J. Am. Ceram. Soc. 91 (2008) 2975–2981.
[10] T. Tsuru, Development of metal-doped silica membranes for increased hydrothermal stability and their applications to membrane reactors for steam reforming of methane, J. Jpn. Petrol. Inst. 54 (2011) 277–286.
[11] D. Uhlmann, S. Smart, J.C. Diniz da Costa, High temperature steam investigation of cobalt oxide silica membranes for gas separation, Sep. Purif. Technol. 76 (2010) 171–178.
[12] H.L. Castricum, A. Sah, R. Kreiter, D.H.A. Blank, J.F. Vente, J.E. ten Elshof, Hydrothermally stable molecular separation membranes from organically linked silica, J. Mater. Chem. 18 (2008) 2150–2158.
[13] R.M. de Vos, W.F. Maier, H. Verweij, Hydrophobic silica membranes for gas separation, J. Membr. Sci. 158 (1999) 277–288.
[14] Q. Wei, Y.-L. Wang, Z.-R. Nie, C.-X. Yu, Q.-Y. Li, J.-X. Zou, C.-J. Li, Facile synthesis of hydrophobic microporous silica membranes and their resistance to humid atmosphere, Microporous Mesoporous Mater. 111 (2008) 97–103.
[15] H.L. Castricum, A. Sah, R. Kreiter, D.H.A. Blank, J.F. Vente, E.J.E. Ten, Hybrid ceramic nanosieves: stabilizing nanopores with organic links, Chem. Commun. (Cambridge, U.K.) (2008) 1103–1105.
[16] M. Kanezashi, K. Yada, T. Yoshioka, T. Tsuru, Organic–inorganic hybrid silica membranes with controlled silica network size: preparation and gas permeation characteristics, J. Membr. Sci. 348 (2010) 310–318.
[17] R.M. de Vos, H. Verweij, High-selectivity, high-flux silica membranes for gas separation, Science 279 (1998) 1710–1711.
[18] H.L. Castricum, G.G. Paradis, M.C. Mittelmeijer-Hazeleger, R. Kreiter, J.F. Vente, J.E. ten Elshof, Tailoring the separation behavior of hybrid organosilica membranes by adjusting the structure of the organic bridging group, Adv. Funct. Mater. 21 (2011) 2319–2329.
[19] H. Qi, J. Han, N. Xu, H.J.M. Bouwmeester, Hybrid organic–inorganic microporous membranes with high hydrothermal stability for the separation of carbon dioxide, ChemSusChem 3 (2010) 1375–1378.
[20] V. Boffa, J.E. ten Elshof, A.V. Petukhov, D.H.A. Blank, Microporous niobia–silica membrane with very low CO_2 permeability, ChemSusChem 1 (2008) 437–443.
[21] G.P. Fotou, Y.S. Lin, S.E. Pratsinis, Hydrothermal stability of pure and modified microporous silica membranes, J. Mater. Sci. 30 (1995) 2803–2808.
[22] M. Kanezashi, M. Sano, T. Yoshioka, T. Tsuru, Extremely thin Pd–silica mixed-matrix membranes with nano-dispersion for improved hydrogen permeability, Chem. Commun. 46 (2010) 6171–6173.
[23] T. Tsuru, R. Igi, M. Kanezashi, T. Yoshioka, S. Fujisaki, Y. Iwamoto, Permeation properties of hydrogen and water vapor through porous silica membranes at high temperatures, AIChE J. 57 (2011) 618–629.
[24] K. Yoshida, Y. Hirano, H. Fujii, T. Tsuru, M. Asaeda, Hydrothermal stability and performance of silica–zirconia membranes for hydrogen separation in hydrothermal conditions, J. Chem. Eng. Jpn. 34 (2001) 523–530.
[25] M.M. Dubinin, L.V. Radushkevich, The equation of the characteristic curve of activated charcoal, Doklady Akademii Nauk SSSR 55 (1947) 327–329.
[26] R.J.R. Uhlhorn, M.H.B.J. Huis In't Veld, K. Keizer, A.J. Burggraaf, Synthesis of ceramic membranes, J. Mater. Sci. 27 (1992) 527–537.
[27] E.J. Kappert, H.J. Bouwmeester, N.E. Benes, A. Nijmeijer, Kinetic analysis of the thermal processing of silica and organosilica, J. Phys. Chem. B 118 (2014) 5270–5277.
[28] H.F. Qureshi, A. Nijmeijer, L. Winnubst, Influence of sol–gel process parameters on the micro-structure and performance of hybrid silica membranes, Journal of Membrane Science 446 (2013) 19–25.
[29] J.B. Miller, E.I. Ko, Control of mixed oxide textural and acidic properties by the sol–gel method, Catal. Today 35 (1997) 269–292.
[30] G.T. Mamott, P. Barnes, S.E. Tarling, S.L. Jones, C.J. Norman, Dynamic studies of zirconia crystallization, J. Mater. Sci. 26 (1991) 4054–4061.
[31] L. Winnubst, P.J. de Veen, S. Ran, D.H.A. Blank, Synthesis and characteristics of nanocrystalline 3Y-TZP and CuO powders for ceramic composites, Ceram. Int. 36 (2010) 847–853.
[32] P. Hacarlioglu, D. Lee, G.V. Gibbs, S.T. Oyama, Activation energies for permeation of He and H2 through silica membranes: an ab initio calculation study, J. Membr. Sci. 313 (2008) 277–283.
[33] R. Kreiter, M. Rietkerk, H. Castricum, H. van Veen, J. ten Elshof, J. Vente, Evaluation of hybrid silica sols for stable microporous membranes using high-throughput screening, J. Sol–Gel Sci. Technol. (2010) 1–8
[34] C.J. Brinker, A.J. Hurd, P.R. Schunk, G.C. Frye, C.S. Ashley, Review of sol–gel thin film formation, J. Non-Cryst. Solids 147–148 (1992) 424–436.
[35] A. Clearfield, P.A. Vaughan, The crystal structure of zirconyl chloride octahydrate and zirconyl bromide octahydrate, Acta Crystallogr. 9 (1956) 555–558.
[36] H. Qi, J. Han, N.P. Xu, Effect of calcination temperature on carbon dioxide separation properties of a novel microporous hybrid silica membrane, J. Membr. Sci. 382 (2011) 231–237.
[37] S. Battersby, S. Smart, B. Ladewig, S. Liu, M.C. Duke, V. Rudolph, J.C.D.d. Costa, Hydrothermal stability of cobalt silica membranes in a water gas shift membrane reactor, Sep. Purif. Technol. 66 (2009) 299–305.

Please cite this article in press as: M. ten Hove et al., Facile synthesis of zirconia doped hybrid organic inorganic silica membranes, Separ. Purif. Technol. (2015), http://dx.doi.org/10.1016/j.seppur.2014.12.033